LFP spectral peaks in V1 cortex: network resonance and cortico-cortical feedback

Kukjin Kang · Michael Shelley ·
James Andrew Henrie · Robert Shapley

Abstract This paper is about how cortical recurrent inter-actions in primary visual cortex (V1) together with feed-back from extrastriate cortex can account for spectral peaks in the V1 local field potential (LFP). Recent studies showed that visual stimulation enhances the γ-band (25–90 Hz) of the LFP power spectrum in macaque V1. The height and location of the γ-band peak in the LFP spectrum were cor-related with visual stimulus size. Extensive spatial summa-tion, possibly mediated by feedback connections from extrastriate cortex and long-range horizontal connections in V1, must play a crucial role in the size dependence of the LFP. To analyze stimulus-effects on the LFP of V1 cortex, we propose a network model for the visual cortex that in-cludes two populations of V1 neurons, excitatory and inhibitory, and also includes feedback to V1 from extrastriate cortex. The neural network model for V1 was a resonant system. The model's resonance frequency (ResF) was in the γ-band and varied up or down in frequency depending on cortical feedback. The model's ResF shifted downward with stimulus size, as in the real cortex, because increased size recruited more activity in extrastriate cortex and V1 thereby causing stronger feedback. The model needed to have strong local recurrent inhibition within V1 to obtain ResFs that agree with cortical data. Network resonance as a consequence of recurrent excitation and inhibition appears to be a likely explanation for γ-band peaks in the LFP power spectrum of the primary visual cortex.

Keywords Visual cortex · LPF · Oscillation · Gamma band · Resonance · Recurrent network

K. Kang (✉)
RIKEN BSI,
Wako, Japan 351-0198
e-mail: kkang@brain.riken.jp

M. Shelley
Courant Institute of Mathematical Sciences, New York University,
New York, NY 10012, USA

M. Shelley · J. A. Henrie · R. Shapley
Center for Neural Science, New York University,
New York, NY 10003, USA

1 Introduction

There has been a lot of scientific investigation of the neural circuit in the primary visual cortex, V1. Experimenters have studied the spatial scales and structural features of synaptic summation in V1 (e.g. Lund 1988; Angelucci et al. 2002; Lund et al. 2003). The temporal dynamics of orientation tuning has been measured (Ringach et al. 1997). Theorists have constructed models for the V1 neural circuit in order to understand orientation selectivity (Ben-Yishai et al. 1995; Somers et al. 1995; Troyer et al. 1998; McLaughlin et al. 2000) and surround suppression (Schwabe et al. 2006).

There also has been extensive investigation of the local field potential (LFP) in V1 cortex (Eckhorn et al. 1988; Gray et al. 1989; Eckhorn et al. 1993; Logothetis et al. 2001; Gieselmann and Thiele 2008). The LFP is usually thought to be an average of cell membrane-potentials near the recording electrode and therefore an index of local synaptic activity in nearby neurons. We measured the visual dependence of the power spectrum of the LFP in V1 when the visual system was stimulated by drifting-grating stimuli. Two significant experimental results were that drifting-grating stimuli selectively enhance the γ-band (25–90 Hz) of the LFP power spectrum even for very small stimuli

(Henrie and Shapley 2005), and that the peak of the power spectrum becomes narrower and moves to lower frequencies for larger grating stimuli (Henrie et al. 2005). More recently, Gieselmann and Thiele (Gieselmann and Thiele 2008).showed that gamma oscillation amplitude increases as the size of stimulus increases.

One natural question is, how can we understand the experimental obserbations of the LFP in terms of the neural circuit in V1? Especially, we need to understand the mechanism for how the size of a visual stimulus is related to γ-band spectral peak in the LFP in V1. In this paper, we study how the power spectrum of neural activity is related to cortical feedback in a model of V1. The model we consider is an elaborated version of a recurrent excitatory-inhibitory network model developed originally to understand orientation selectivity within a single V1 hypercolumn (Kang et al. 2003). We report here that power spectral peaks occur in the V1 model as a consequence of resonance in the local network. Resonance often is observed in recurrent excitatory-inhibitory networks and has been invoked before as a possible source of γ-band peaks (Freeman 1975; Leung 1982; Rennie et al. 2000). Another new theoretical result is that, in the V1 model, feedback from extrastriate cortex sharpens the power spectrum of neural activity by excitatory feedback. The model's local inhibitory feedback loop increases, and its excitatory feedback loop decreases, the resonance frequency ResF.

Stronger γ-band peaks with larger drifting-grating stimuli (Henrie et al. 2005) can be explained in our model by the effect of neuronal thresholds on the effective strength of feedback. With different parameters, the V1 model offered in this paper can cause cortical sharpening of orientation selectivity either as a Mexican hat in the orientation domain (Kang et al. 2003) or in an inhibition-dominated regime (Ben-Yishai et al. 1995; Kang et al. 2003). We found that the inhibition-dominated scenario is more likely because the ResF of the Mexican-hat scenario is too low to be consistent with LFP data.

Here is an outline of the paper. Section I shows that resonance in the γ-band occurs in a recurrent excitatory-inhibitory neural network model without 2D structure, and then offers a calculation of the ResF and damping time constant, τ_{damp}, for this unstructured model. Section II introduces the network model of V1. Then in Section III, based on the analytical results on the unstructured model in Section I, we study the ResF and τ_{damp} of the V1 model without extrastriate cortex feedback and ignoring threshold nonlinearity. In Section IV, we study how the ResF and τ_{damp} depend on the feedback from extrastriate cortex., In Section V, we investigate the effect of threshold nonlinearity. The Discussion, Section VI, relates the present work to previous experimental and theoretical studies of γ-band activity and of V1 function.

Neural network without 2D structure Before we consider a model of the neural circuit in V1, we consider a simple neural network whose 2D connectivity is unstructured (that is, all-to-all and isotropic) and for which the power spectrum can be calculated analytically. In Section III we show that our V1 model with 2D structure can be reduced to a network model similar to this simpler case if a spatial average is taken and several relevant conditions are met. It should be emphasized that we do not consider spontaneous oscillation with bifurcation but consider oscillations generated by resonance and noise in this paper.

Consider a population of asynchronous excitatory and inhibitory neurons interacting with each other through synaptic connections. The rate functions $m(t)$ and $n(t)$ are the low-pass filtered presynaptic firing rates of excitatory and inhibitory neuronal populations with synaptic conductance time constants τ_E and τ_I, respectively. The conductance rate variables, $m(t)$ and $n(t)$, for excitatory and inhibitory populations respectively, evolve according to a standard neural model (Kang et al. (2003); for the derivation of the rate model from a spiking model, see Appendix A), and obey the differential equations:

$$\tau_E \frac{dm}{dt} = -m + [S_{EIE}m - S_{EI}n + I_E]$$
$$\tau_I \frac{dn}{dt} = -n + [S_{IE}m - S_{II}n + I_I] \qquad (1.0)$$

where I_E and I_I are the excitatory LGN synaptic inputs to the excitatory and inhibitory populations, respectively. The parameters S_{EE} and S_{EI} are respectively the efficacies of excitatory and inhibitory synaptic connections to a postsynaptic excitatory neuron, while S_{IE} and S_{II} are respectively the efficacies of excitatory and inhibitory synaptic connections to a postsynaptic inhibitory neuron. While we do not do so here, a rectifying or sigmoidal nonlinearity could be introduced and would act upon the terms in brackets. Here we consider a linearized approximation ignoring rectification nonlinearity for analytical calculation of ResF and damping constant, τ_{damp}, and rewrite the network equations in the following form.

$$\frac{d\mathbf{x}}{dt} = -\mathbf{A}\mathbf{x} + \mathbf{b}(t) \qquad (1.1)$$

where $\mathbf{x}(t) = (m(t), n(t))^T$,

$$\mathbf{A} = \begin{pmatrix} (1 - S_{EE})/\tau_E & S_{EI}/\tau_E \\ -S_{IE}/\tau_I & (1 + S_{II})/\tau_I \end{pmatrix} \qquad (1.2)$$

$$\mathbf{b} = \begin{pmatrix} I_E(t)/\tau_E \\ I_I(t)/\tau_I \end{pmatrix}. \qquad (1.3)$$

The solution of Eq. 1.1 has the form $\exp(-\mathbf{A}t)\mathbf{x}_0 + \int ds \exp(-\mathbf{A}(t-s))\mathbf{b}(s)$ with the temporal power spectra

of $m(t)$ and $n(t)$ peaking at ResF, v_0. The eigenvalues of the matrix A have the form $1/\tau_{damp} \pm 2\pi v_0 i$ where τ_{damp} is the damping time constant of oscillation. Both τ_{damp} and v_0 are calculated analytically to be

$$\tau_{damp} = 2/((1 - S_{EE})\tau_E^{-1} + (1 + S_{II})\tau_I^{-1}) \quad (1.4)$$

$$v_0 = \sqrt{Z_0}/2\pi \quad \text{if} \ Z_0 > 0 \quad (1.5)$$

$$v_0 = 0 \quad \quad \text{if} \ Z_0 \leq 0$$

where

$$Z_0 = \tau_E^{-1}\tau_I^{-1}S_{IE}S_{EI} - \left(\tau_E^{-1}(1 - S_{EE}) - \tau_I^{-1}(1 + S_{II})\right)^2/4. \quad (1.6)$$

Consider the power spectrum of $m(t)$ in Eq.1.1 when the visual cortex is stimulated by a continuously drifting grating pattern (Fig. 1). We make the approximation that $I_E(t)$ and $I_I(t)$ are Gaussian white noise inputs of equal variance, uncorrelated with each other. By using Fourier transformation and algebraic rearrangement, one can derive the following expression for the power spectrum:

$$\left\langle |\tilde{m}(w)|^2 \right\rangle = \frac{\left((1 + S_{ii})^2 + \tau_i^2 w^2\right)\left\langle \left|\tilde{I}_E(w)\right|^2 \right\rangle + S_{EI}^2 \left\langle \left|\tilde{I}_I(w)\right|^2 \right\rangle}{\tau_E^2 \tau_I^2 \left(\left(\tau_{damp}^{-2} + 4\pi^2 v_0^2 - w^2\right)^2 + 4\tau_{damp}^{-2}w^2\right)} \quad (1.7)$$
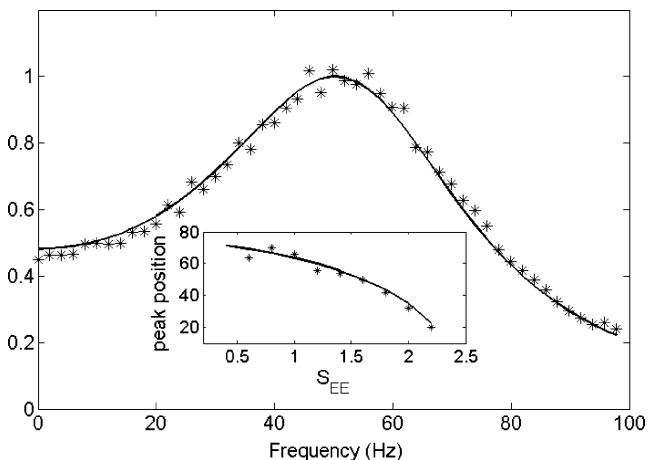

Fig. 1 Normalized power spectrum of $m(t)$, the excitatory neurons' conductance rate, and its dependence on recurrent excitation strength S_{EE}. The solid line is the power spectrum calculated using Eq. 1.7. * markers show the spectrum calculated from numerical integration of Eq. 1.1 with S_{EE}=1.5, S_{EI}=1, S_{IE}=4, S_{II}=2. τ_E=3 msec and τ_I= 6 msec. The inset shows the position of the power spectrum peak for different values of the recurrent excitatory coupling strength, S_{EE}. In the inset also, the solid line shows the peak position of the power spectrum calculated using Eq. 1.7. * markers show the results of numerical integration of Eq. 1.1
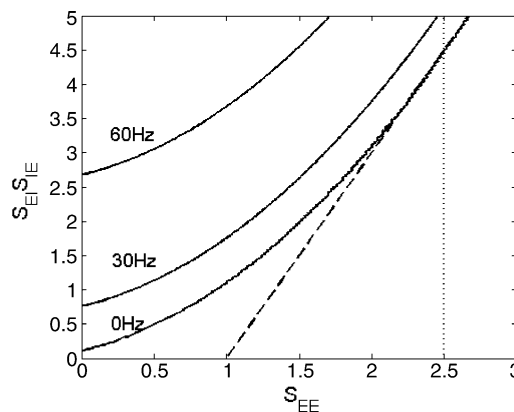

Fig. 2 A contour plot of ResF and the stability boundary. Curved lines with numbers on them are contour lines for ResF. A dashed line and a dotted line are for stability conditions. $(1 - S_{EE})(1 + S_{II}) + S_{EI}S_{IE} > 0$(dashed) and $S_{EE} < 1 + \tau_E(1 + S_{II})/\tau_I$ (dotted). τ_E= 3 msec and τ_I=6 msec. S_{II}=2

$\tilde{f}(w)$ is the Fourier transformation of $f(t)$, where $\langle \ldots \rangle$ is the average over many different realizations of feed-forward input, $I_E(t)$ and $I_I(t)$. The power spectrum peaks at $w \cong 2\pi v_0$ when the damping time constant τ_{damp} is large (Fig. 1) because the denominator of Eq. 1.7 has a minimum at $w^2 = 4\pi^2 v_0 - \tau_{damp}^{-2}$.

Another way to calculate the power spectrum of $m(t)$ is to integrate Eq. 1.1 numerically. Numerical integration was done here just to emphasize that we have two different ways to study the power spectrum in this neural network model. Since an exact result is available, numerical integration does not provide a new result, here. But we do numerical study in Section V for a model in which analytic calculation is not possible. The numerical integration results are also displayed in Fig. 1 and agree with the analytic calculation.

Figure 1 also shows the positions of the power spectrum peak for various values of S_{EE} calculated from Eq. 1.7 and numerically, in the inset. For small S_{EE}, the estimation of the peak position is somewhat less accurate because the power spectrum is broad. Figure 1's inset demonstrates that the ResF of the recurrent excitatory-inhibitory network decreases with increasing recurrent excitatory coupling.

The resonant frequency v_0 is determined by the strengths of three feedback loops: S_{EE}, S_{II} and $S_{EI}S_{IE}$. Figure 2 shows constant-frequency contours of v_0 as a function of S_{EE} and $S_{EI}S_{IE}$ for τ_E=3, τ_I=6 msec and S_{II}= 2, while Fig. 3 shows constant-frequency contours of v_0 as a function of S_{II} and $S_{EI}S_{IE}$ for τ_E=3, τ_I=6 msec and S_{EE}=1.

The first term of Eq. 1.6 shows that resonance occurs in this unstructured model even with only the inhibitory loop between excitatory and inhibitory neurons present, so that inhibitory neurons are excited by excitatory neurons and excitatory neurons are inhibited by inhibitory neurons. The excitatory-inhibitory feedback loop is essential in generating
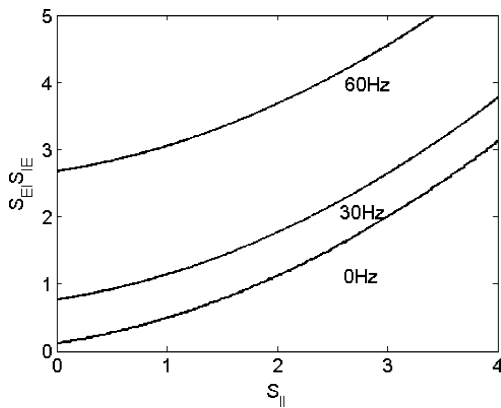
Fig. 3 A contour plot of ResF . Curved lines with numbers on them are contour lines for ResF. τ_E=3 msec and τ_I=6 msec. S_{EE}=1. Stability conditions are met for all the points in the plot

oscillation. The resonant frequency v_0 is zero for $S_{EI}S_{IE}$=0. v_0 increases monotonically with increasing $S_{EI}S_{IE}$ when v_0>0.

The damping constant τ_{damp} is independent of $S_{EI}S_{IE}$. The resonance frequency v_0 tends to decrease due to self-excitatory and self-inhibitory feedback loops because the effect of $S_{EI}S_{IE}$ inhibition is weakened by these feedback loops. Speaking more precisely, v_0 decreases as the self-inhibitory feedback strength, S_{II} increases unless S_{II} is very small: when $S_{II} > -1 + \tau_I(1 - S_{EE})/\tau_E = 1 - 2S_{EE}$, v_0 decreases as S_{II} increases. When $S_{EE} > 1 - \tau_E(1 + S_{II})/\tau_I = 0.5 - 0.5S_{II}$, v_0 decreases as S_{EE} increases. In these calculations we assumed the synaptic time constant for inhibition was twice that for excitation.

There are two conditions for dynamical stability. The first is that $D = (1 - S_{EE})(1 + S_{II}) + S_{EI}S_{IE} > 0$. The discriminant D determines the cortical gain with the population firing rates diverging when D≤0. The second stability condition is that $S_{EE} < 1 + \tau_E(1 + S_{II})/\tau_I$. This condition can be written as τ_{damp}>0. When the second stability condition is violated, oscillation amplitudes grow without limit.

2 A model of the V1 neural network

We model the cortical circuitry in V1 cortex by two populations of excitatory and inhibitory neurons interacting with each other in a two-dimensional plane. Our model also has another population of excitatory neurons representing neurons in extrastriate cortex receiving input from V1 excitatory neurons and sending feedback to V1. When you take into account the spatial scale of synaptic summation and the size of stimuli in the experiments of Henrie and Shapley (Henrie and Shapley 2005), it is crucial to include in the model long-range synaptic connections such as those between an extrastriate cortex layer and V1 and also long range horizontal connections within V1 in order to

reproduce the experimental observations.. Local isotropic synaptic connections are too short. A similar model of V1 without the extrastriate cortex feedback was used in a previous study of the orientation tuning of neurons in V1 (Kang et al. 2003). Figure 4 is a schematic view of our model. In this model, feedforward input from V1 to extrastriate cortex is only from excitatory neurons, following anatomical observations (e.g. Angelucci et al. 2002). Just for the sake of simplicity, we made the approximation that extrastriate cortex has only excitatory neurons (see Discussion).

A set of mean-field rate model equations with $m(\vec{r},t)$, $n(\vec{r},t)$ and $o(\vec{r},t)$ as the dynamic variables describes the network dynamics (Kang et al. 2003). V1 excitatory cells located at the two-dimensional cortical coordinate $\vec{r}$ generate the synaptic conductance rate $m(\vec{r},t)$ (normalized by the peak conductance). $n(\vec{r},t)$, and $o(\vec{r},t)$ are synaptic conductance rates similarly defined for inhibitory cells in V1, and excitatory cells in extrastriate cortex, respectively. Dynamic equations for these three populations of neurons are

$$\tau_E \frac{dm(\vec{r},t)}{dt} = -m(\vec{r},t) + [I_{LGN}(\vec{r},t) + S_{EE}K_{EE}*m(\vec{r},t) - S_{EI}K_{EI}*n(\vec{r},t) + U_{EF}K_{EF}*o(\vec{r},t) - T_E]_+$$
(2.1)

$$\tau_I \frac{dn(\vec{r},t)}{dt} = -n(\vec{r},t) + [I_{LGN}(\vec{r},t) + S_{IE}K_{IE}*m(\vec{r},t) + U_{IF}K_{IF}*o(\vec{r},t) - T_I]_+$$
(2.2)

$$\tau_{EE} \frac{do(\vec{r},t)}{dt} = -o(\vec{r},t) + [U_{FE}K_{FE}*m(\vec{r},t) - T_O]_+$$
(2.3)

In Eqs. 2.1–2.3, $[..]_+$ is the notation for a simple rectification nonlinearity, where [x]=x for x>0, and [x]=0 for x<0. Hence, T_E,T_I and T_0 are threshold parameters for excitatory neurons in V1, inhibitory neurons in V1, and excitatory neurons in the extrastriate cortex, respectively.
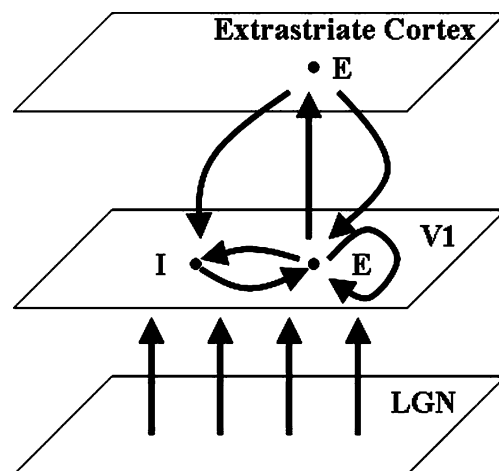

Fig. 4 Schematic view of a model for V1 neural circuitry. E (I) represents excitatory (inhibitory) neurons

The term I_{LGN} in Eqs. 2.1 and 2.2 represents the LGN drive for excitatory and inhibitory populations. The function $K_{PP'}\left(\overrightarrow{r},\overrightarrow{r}'\right)$ denotes the (normalized) spatial profile of cortical interactions. The kernels K_{PP} are normalized to have unit sums so that S_{PP} denote the total strength of synaptic connection to P type cells from P' type cell ($P=E,I$ and F; E and I represent excitatory and inhibitory neurons in V1, respectively; F represents excitatory neurons in extrastriate cortex). For example, the term $K_{EE}*m\left(\overrightarrow{r},t\right) = \sum_{\overrightarrow{r}'} K_{EE}\left(\overrightarrow{r},\overrightarrow{r}'\right)m\left(\overrightarrow{r}',t\right)$ denotes cortical feedback from excitatory to excitatory neurons in V1. For the synaptic connections related to extrastriate cortex, we use the symbol U_{PP} instead of S_{PP}. Extrastriate neurons do not receive direct LGN input in the model as in the biological cortex. The feedback from extrastriate cortex excites both excitatory and inhibitory neurons in V1, based on the results of Gonchar and Burkhalter (2003).

The synaptic connections of our model can be grouped into three classes. The first class is that of local isotropic connections between neurons in V1 (Kang et al. 2003; McLaughlin et al. 2000). The second class is that of long range horizontal connections within V1. The third class is that of feedback connections from extrastriate cortex, which are known to have a longer range of visual, spatial summation (Angelucci et al. 2002).

The spatial profile of the strength of isotropic synaptic connections such as local V1 connections may be modeled with normalized two-dimensional Gaussian functions of cortical distance $\left|\overrightarrow{r}-\overrightarrow{r}'\right|$ as they were in previous studies (Kang et al. 2003; Tao et al. 2006): $K_{PP'}\left(\overrightarrow{r},\overrightarrow{r}'\right) = G\left(\overrightarrow{r},\overrightarrow{r}',\sigma_{PP'}\right)$ where $G\left(\overrightarrow{r},\overrightarrow{r}',\sigma_{PP'}\right)$ is a 2D Gaussian distribution with variance, $\sigma_{PP'}^2$.

The strengths of long-range horizontal synaptic connections are known to depend on the difference of preferred orientation, $\theta\left(\overrightarrow{r}\right)$ and we may model the spatial profile of the connections as a product of a Gaussian distribution with a cosine function (Goldberg et al. 2004).

$$K_{pp'}^{long}\left(\overrightarrow{r},\overrightarrow{r}'\right) = \frac{1}{G}e^{-\frac{\left|\overrightarrow{r}-\overrightarrow{r}'\right|^2}{2\sigma_K^2}}\left(1+\cos\left(\left(2\theta\left(\overrightarrow{r}\right)-\theta\left(\overrightarrow{r}'\right)\right)\right)\right)$$
(2.4)

where G is a normalization constant. These long-range synaptic connections are known to be excitatory.

S_{IE} and S_{EE} consist of two parts.

$$S_{IE} = S_{IE}^{short} + S_{IE}^{long}$$
(2.5)

$$K_{IE} = \left(K_{IE}^{short}S_{IE}^{short} + K_{IE}^{long}S_{IE}^{long}\right)/S_{IE}$$
(2.6)

$$S_{EE} = S_{EE}^{short} + S_{EE}^{long}$$
(2.7)

$$K_{EE} = \left(K_{EE}^{short}S_{EE}^{short} + K_{EE}^{long}S_{EE}^{long}\right)/S_{EE}$$
(2.8)

The LGN afferent input to a neuron is specified by its preferred orientation (PO), i.e., by its location within the pinwheel orientation map in the V1 plane, shown in Fig. 5. The 2D coordinate $\overrightarrow{r}$ in the V1 plane is represented in polar coordinates $\overrightarrow{r} = r(\cos\theta,\sin\theta)$ where the origin is the closest pinwheel center. The PO of a cell ranges from 0 to 180 degrees and is equal to one half of its polar angle, in the cortical map as in Fig. 5. The LGN input is modeled as $I_{LGN}\left(\overrightarrow{r},t\right) = (A + B\cos(\theta-2\theta_0)+\eta(t))sf\left(\overrightarrow{r}\right)$ where A is the mean LGN input to the cortical cell, and B is its orientation modulation amplitude and θ_0 is the orientation of the stimuli. The function $\eta(t)$ is white noise. The function $sf\left(\overrightarrow{r}\right)$ is 1 if the stimulus activates LGN neurons at $\overrightarrow{r}$, and is 0 otherwise.

3 ResF of the V1 model for the uniform mode

We calculate ResF and τ_{damp} of the V1 model in this section, ignoring the rectification nonlinearity of spike firing threshold, and averaging conductance rates over $\overrightarrow{r}$. In Section V we will calculate the power spectrum of the neural activity by numerically integrating Eqs. 2.1–3 including the rectification nonlinearity that we are neglecting in analytical calculations. The parameter sets for such numerical integrations are chosen based on the analytic results.

Note that

$$\int d\overrightarrow{r}d\overrightarrow{r}'K_{PP'}\left(\overrightarrow{r},\overrightarrow{r}'\right)m\left(\overrightarrow{r}',t\right)$$

$$= \int d\overrightarrow{r}'\left(\int d\overrightarrow{r}K_{PP'}\left(\overrightarrow{r},\overrightarrow{r}'\right)\right)m\left(\overrightarrow{r}',t\right)$$

$$= \int d\overrightarrow{r}m\left(\overrightarrow{r},t\right).$$
(3.1)
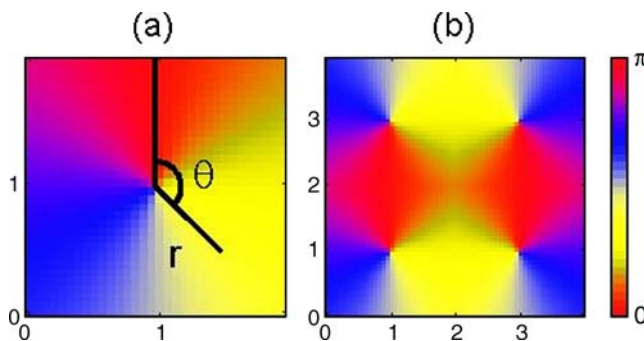

Fig. 5 Pinwheel architecture in the model. (a): a single pinwheel system. Each cell is indexed by its distance r from the pinwheel center at (1,1), and an angle θ measured relative to the depicted vertical line. The preferred orientation of the cell is $\theta/2$. (b): four pinwheel system, with centers at (1,1), (1,3), (3,1), and (3,3). Θ of each cell is defined relative to the nearest center. The red regions show the two horizontal columns – each connecting center pairs with opposite parity

Equation 3.1 is a consequence of the fact that $K_{PP'}$ $\left(\overrightarrow{r}, \overrightarrow{r'}\right)(P, P' = E, I \text{ and } F)$ are normalized. We integrate both sides of Eqs. 2.1–3 over space to convert them into dynamic equations of space-averaged variables:

$$\frac{d}{dt}\begin{pmatrix}\widehat{m} \\ \widehat{n} \\ \widehat{o}\end{pmatrix} = -A\begin{pmatrix}\widehat{m} \\ \widehat{n} \\ \widehat{o}\end{pmatrix} + B \tag{3.2}$$

where

$$A = \begin{pmatrix} \tau_E^{-1}(1 - S_{EE}) & \tau_E^{-1}S_{EI} & -\tau_E^{-1}U_{EF} \\ -\tau_I^{-1}S_{IE} & \tau_I^{-1}(1 + S_{II}) & -\tau_I^{-1}U_{IF} \\ -\tau_{EE}^{-1}U_{FE} & 0 & \tau_{EE}^{-1} \end{pmatrix} \tag{3.3}$$

$$B = \begin{pmatrix} \tau_E^{-1}\widehat{I}_{LGN} \\ \tau_I^{-1}\widehat{I}_{LGN} \\ 0 \end{pmatrix} \tag{3.4}$$

Here $\widehat{f} = \int f\left(\overrightarrow{r}\right)d\overrightarrow{r}$ so that $\widehat{I}_{LGN}$ is the space-averaged LGN input.

Note that the details of the spatial profile of synaptic connections are not important in deriving Eq. 3.2 and determining the ResF of the spatially averaged neural activity. Whether the synaptic connection is patchy or isotropic, the oscillation frequency is the same. Only total strengths are important in Eq. 3.2. Later, we show how a threshold nonlinearity makes the difference (Section V).

When the strength of synaptic connections are symmetrical with respect to two positions in the neural network and the dynamic equations are linear, as we assumed in this section, the spatial activity pattern can be decomposed into orthogonal eigenmodes and the evolution of each eigenmode can be handled separately. Equations 3.2–4 are the dynamic equations of this uniform mode derived from Eqs. 2.1–3. without rectification nonlinearity.

For given spatial profiles of synaptic connections, there are many other non-uniform eigenmodes and these modes may oscillate with different ResFs and τ_{damp} s. But we consider only the uniform mode in this paper for two related reasons. First, we want to study how the LFP power spectrum is related to cortical feedback. The uniform mode is the spatially averaged conductance rate, which is assumed to be proportional to LFP. Second, spatially fluctuating components of the feedback activity pattern should be averaged out and disappear because the feedback from extrastriate cortex has a broad spatial profile. These considerations suggest that the resonance effects of the uniform mode, or in other words spatially-coherent feedback, is important in V1. Equations 3.2–4 are the dynamic equations of this uniform mode derived from Eqs. 2.1–3 when we make approximation that there is no rectification nonlinearity.

Before we study the effect of the feedback from extrastriate cortex, consider a simpler case without the feedback from extrastriate cortex. When the feedback from extrastriate cortex does not exist ($U_{PP}=0$), V1 and extrastriate cortex are decoupled and the dynamic equations are identical with Eq. 1.1. The ResF and damping time constant are already studied in Section I and given by Eqs. 1.4–6.

4 ResF with feedback from extrastriate cortex

Here, we focus on how feedback from extrastriate cortex changes the power spectrum of the neural activity in our model. Feedback from higher levels of information processing is ubiquitous in the brain. For example, LGN receives massive feedback connections from V1 while V1 receives feedback from extrastriate cortex with a broad spatial profile (Angelucci et al. 2002).

The feedback from extrastriate cortex increases or decreases the ResF depending on whether the feedback is to inhibitory neurons or excitatory neurons. The extrastriate cortex feedback increases τ_{damp} and thereby sharpens the peak of the power spectrum in both cases.

When there is feedback from extrastriate cortex $U_{PP}\neq 0$, the extrastriate layer and V1 layer are dynamically coupled and eigenvalues of the matrix in Eq. 3.3 can be calculated. The result of the calculation are given in Fig. 6 which shows how the feedback from extrastriate cortex changes the ResF for given S_{EE}, $S_{EI}S_{IE}$ and S_{II}. Increasing the excitatory feedback, $U_{FE}U_{EF}$, tends to decrease the ResF of the network and increasing the inhibitory feedback, $S_{EI}U_{IF}U_{FE}$, increases the ResF. The 80 Hz contour line from the origin in Fig. 6 is where the two opposing effects cancel each other in this example. Note that the ResF at the
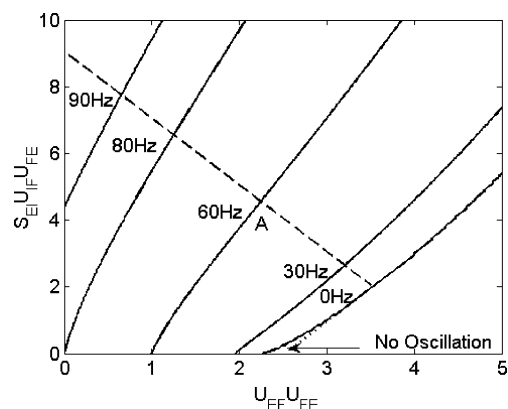

Fig. 6 Contour plot of ResF for the model with extrastriate feedback. $S_{EE}=1$, $S_{EI}S_{IE}=5.05$, $S_{II}=1$. $\tau_E=\tau_{EE}=3$ msec and $\tau_I=6$ msec. Solid lines with numbers are contour lines. The dashed line is the stability line given by Eq. 4.4. The dotted line is the stability line given by Eq. 4.3. The ResF is 80 Hz at the origin

origin of Fig. 6 is the ResF of our model without the extrastriate cortex. The extrastriate cortex increases ResF in the area above the 80 Hz contour line. The extrastriate cortex decreases ResF in the area below the 80 Hz contour line.

There is no general analytic expression of the ResF for the model with extrastriate cortex feedback, and it must be calculated by calculating eigenvalues of the matrix in Eq. 3.3 numerically. But analytic expressions of $v =$ ResF as a function of strengths of feedback loops are calculable analytically in several special cases. For example, when $\tau_{damp} = \infty$, v is (see Appendix B for the derivation),

$$(2\pi v)^2 = \left(T + \tau_{EE}^{-1}\right)^{-1} \tau_E^{-1} \tau_I^{-1} \tau_{EE}^{-1} \qquad (4.1)$$
$$\left(D + S_{EI} U_{IF} U_{FE} - (1 + S_{II}) U_{FE} U_{EF}\right)$$

where

$$T = \tau_E^{-1}(1 - S_{EE}) + \tau_I^{-1}(1 + S_{II})$$

and

$$D = (1 - S_{EE})(1 + S_{II}) + S_{EI} S_{IE}.$$

Excitatory feedback, $U_{FE} U_{EF}$, decreases v, and inhibitory feedback, $S_{EI} U_{IF} U_{FE}$, increases v in Eq. 4.1.

Finally, the ResF of the network is reducible to the resonant frequency without feedback, v_0, when the synaptic time constant for the feedback from extrastriate cortex, τ_{EE}, is large. Figure 7 shows the ResF for τ_{EE}=60 msec. The NMDA receptor has such a long decay time constant. Note in Fig. 7 that contour lines of ResF are nearly vertical showing that the ResF is only very weakly affected by the feedback loop from the extrastriate cortex. With a large synaptic time constant, the feedback from extrastriate cortex does not change ResF and τ_{damp} but the non-oscillatory component of firing rate is changed by the
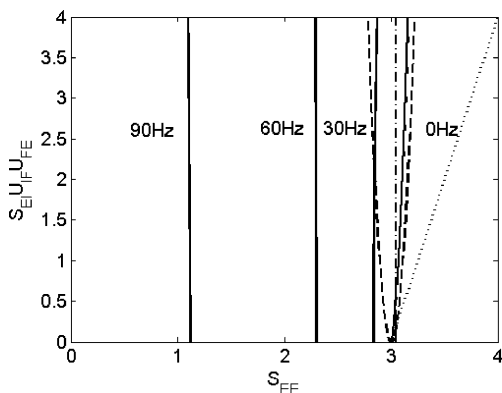

Fig. 7 Contour plot of ResF when extrastriate feedback time constant is large. $S_{EI}S_{IE}$=8, S_{II}=3. $U_{EF}U_{FE}$=0 τ_E=3 msec, τ_I=6msecs and τ_{EE}= 60 msec. Solid lines with numbers are contour lines. The dash-and-dot line is stability line given by Eq. 4.2. The dotted line is the stability line given by Eq. 3.10. The dashed line is stability line given by Eq. 4.4
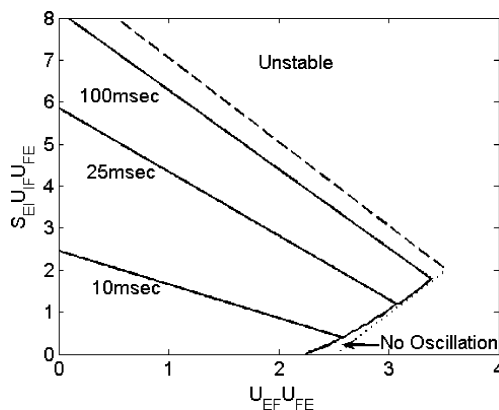

Fig. 8 Contour plot of damping time, τ_{damp}, as a function of feedback strength. S_{EE}=1, $S_{EI}S_{IE}$=5.05, S_{II}=1.τ_E=τ_{EE}=3 msec and τ_I=6 msec. Solid lines with numbers are contour lines for damping time constant, τ_{damp}. The dashed line is the stability line given by Eq. 4.4. The dotted line is the stability line given by Eq. 4.3. There is no oscillation below the curved solid line labeled "No Oscillation"

feedback. This observation implies that if feedback perturbs the LFP spectrum in the γ-band, it must do so via fast (presumably AMPA) excitatory feedback.

τ_{damp} is given by the inverse of the real part of the eigenvalue of A in Eq. 3.3. and determines the width of the power spectrum peak. We found that τ_{damp} diverges and oscillation amplitude grows without limit when the feedback from extrastriate cortex is strong. This is so even when the excitatory feedback from extrastriate cortex is only to inhibitory neurons in V1. Figure 8 shows how τ_{damp} depends on the strengths of the feedback from extrastriate cortex. τ_{damp} is small at the origin and the peak of the power spectrum is sharpened by the feedback from extrastriate cortex. For example, when the inhibitory feedback loop strength, $S_{EI}U_{IF}U_{FE}$, increases, the real parts of complex eigenvalues decrease, and the oscillation damps with a longer time constant, τ_{damp}.

The behavior of the V1 model with feedback can be studied systematically through its stability conditions (see Appendix B for the derivation of these conditions).

$$\tau_E^{-1}(1 - S_{EE}) + \tau_I^{-1}(1 + S_{II}) + \tau_{EE}^{-1} > 0 \qquad (4.2)$$

$$(1 - S_{EE} - U_{FE}U_{EF})(1 + S_{II}) + S_{EI}S_{IE} + S_{EI}U_{IF}U_{FE} > 0, \qquad (4.3)$$

$$T\left(\tau_E^{-1}\tau_I^{-1}D + \tau_{EE}^{-1}T + \tau_{EE}^{-2}\right) - \tau_E^{-1}\tau_I^{-1}\tau_{EE}^{-1}S_{EI}U_{IF}U_{FE}$$
$$- \tau_E^{-1}\tau_{EE}^{-1}\left(\tau_{EE}^{-1} + \tau_E^{-1}(1 - S_{EE})\right)U_{EF}U_{FE} > 0. \qquad (4.4)$$

The network is unstable when self-excitation S_{EE} (Eq. 4.2) is too strong. The discriminant (see the end of Section I) should be positive for the network to be stable (Eq. 4.3). These two conditions restrict mainly the strengths of the self-excitatory feedback, S_{EE}, and the excitatory

feedback loop from extrastriate cortex, $U_{FE}U_{EF}$. The condition of Eq. 4.4 is related to the stability of oscillation and restricts the strength of the inhibitory feedback loop, $S_{EI}U_{IF}U_{FE}$. When it is violated, the oscillation amplitude of the firing rate grows without limit. Note that without feedback from extrastriate cortex, the first term in Eq. 4.4 is positive when the network is stable.

5 ResF and stimulus size

Here, we show that ResF depends on the size of visual stimulus because of the effect of threshold nonlinearity. We calculate the power spectra for the full nonlinear V1 model (Eqs. 2.1–3, including rectification) for stimuli with various sizes to study how stimulus size affects the γ-band peak in the power spectrum. We estimate the power spectrum of neural activity in our V1 model by numerically integrating Eqs. 2.1–3 using a 4th-order Runge-Kutta integration method. We chose LGN input and threshold values such that V1 neurons without feedforward LGN input, and extrastriate neurons without strong feed-forward input from V1, were inactive because of spike-firing thresholds.

We need an additional approximation for this numerical calculation. It is difficult to integrate the dynamic equations numerically for a model with long-range patchy connections because such calculations are very slow for a model with many hypercolumns. For the model with an isotropic Gaussian spatial kernel, synaptic summation could be calculated using the FFT but this is not possible for the model with horizontal connections in which synaptic connections depend on the preferred orientation as well as cortical distance.

Here we omit patchy long range horizontal connections in V1 and assume that the long range connections from extrastriate cortex are isotropic. This is an unrealistic simplification but allows two important conclusions to be made by means of a numerical calculation. First, ResF of the neural network is changed little by the threshold nonlinearity when the visual stimulus is full field. The power spectrum is significantly different from the linear case only when population activity is subthreshold over most of the stimulated area. Second, we found that the peak position of the power spectrum changed from v_0 of Section I to v of Section III as the size of stimulus increased because the threshold nonlinearity changes effective strengths of feedback loops. This result suggests that a qualitatively similar change should happen in the original model with patchy long-range horizontal connections and that the observation of Henrie et al. (2005) on the stimulus-size dependence of the γ-band peak can be explained in terms of the recurrent V1 network with feedback from extrastriate cortex, including neuronal thresholds.

As the stimulus size increases from 40 to 160 (the unit of area is the area of a single hypercolumn which we assume to be $4 \times 10^4 \, \mu m^2$), the peak of the power spectrum changes in a graded manner from $v_0 = 103 \, Hz$ in Section I to $v = 42 \, Hz$ from Section III, as shown in Fig. 9. This roughly matches the experimental observation of Henrie et al. (2005). We used v_0, v and τ_{damp} as guidelines to choose parameter values for the simulation. The strengths of synaptic connections are $S_{EE} = 1$, $S_{EI}S_{IE} = 8$, $S_{II} = 1$, $U_{EF}U_{FE} = 4$ and $S_{EI}U_{IF}U_{FE} = 3$ in the simulation shown in Fig. 9. We assume that $\sigma_{EE} = \sigma_{IE} = 0.5$. $\sigma_{EI} = \sigma_{II} = 0.45$. $\sigma_{FE} = \sigma_{EF} = \sigma_{IF} = 3$ where the length scale is the radius of a hypercolumn which is about $100 \, \mu m$. The results of numerical calculation were not sensitive qualitatively to the power of the white noise used in the simulations.

The local inhibitory feedback, with $S_{EI}S_{IE} = 8$, is larger than local excitatory feedback $S_{EE} = 1$ in order to obtain a large value of v_0, as in the cortical data. With the strength of local synaptic connections within V1 fixed, we choose a point in a phase diagram similar to that in Fig. 6 to decide the feedback strengths for extrastriate cortex, taking into consideration also the values of v and τ_{damp}. To make τ_{damp} large, we choose values of U_{EF}, U_{IF} so that the network is at a point in the phase plane close to a stability line like the one given by Eq. 4.4; v is about 40 Hz there. It turns out that the strengths of excitatory feedback and inhibitory feedback loops from extrastriate cortex are nearly balanced. This is the result of the two constraints given by v and τ_{damp}.

The peak of the LFP power spectrum in Fig. 9 moves to lower frequencies and becomes sharper in this parameter
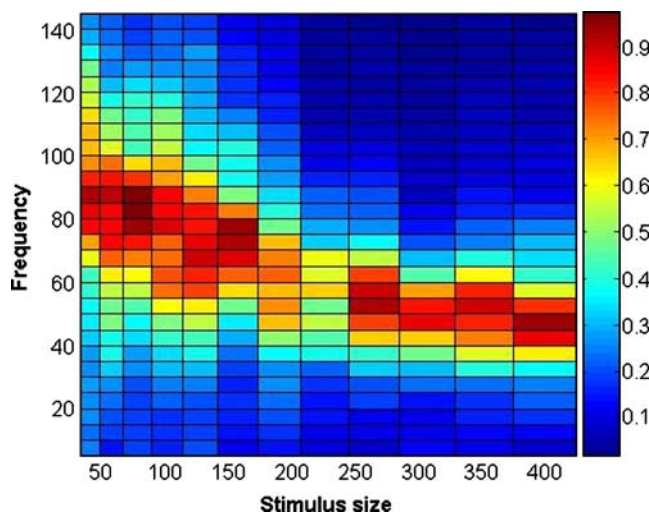

Fig. 9 A 2D plot of the normalized Power spectrum of $m(t)$ for various sizes of stimulus. The unit of the stimulus size is the area of single hypercolumn. $S_{EE} = 1$, $S_{EI}S_{IE} = 8$, $S_{II} = 1$. $U_{EF}U_{FE} = 4$ and $S_{EI}U_{IF}U_{FE} = 3$. $\tau_E = 3$ msecs, $\tau_I = 6$ msecs and $\tau_{EE} = 3$ msecs. $\sigma_{EE} = \sigma_{IE} = 0.5$. $\sigma_{EI} = \sigma_{II} = 0.45$. $\sigma_{FE} = \sigma_{EF} = \sigma_{IF} = 3$. Power spectrum is normalized by the largest value and the bar at right side shows the normalized powers in a color scale

regime as stimulus size increases because $v_0 > v$ and τ_{damp} become larger when there is extrastriate feedback (see Figs. 6 and 8). The peak of the V1 power spectrum may move either to lower or higher frequencies, depending on the relative amount of feedback onto excitatory and inhibitory neurons in the local circuit. The dependence of ResF on stimulus size is present in the nonlinear model but not in the linearized model analyzed in Section IV.

The result in Fig. 9 can be understood in terms of effective strengths of total feedback connections. The strengths of total feedback synaptic connections depend on the size of the stimulus because of the threshold non-linearity in the model. For a small stimulus, only neurons in a small area of extrastriate cortex are active and the feedback connections from inactive extrastriate neurons do not return feedback. Figure 10 shows a schematic view of a neuron in V1 summing up synaptic inputs from extrastriate cortex. The gray area represents a population of neurons activated by a visual stimulus.

The change of the power spectrum with stimulus size depends crucially on the spatial profile of synaptic connections. There are two different kinds of synaptic connections in our mode used in this Section l: short range V1 connections and long-range synaptic connections from and to extrastriate cortex. For a stimulus whose size is smaller than the spatial extent of convergent excitatory input onto extrastriate neurons, the ResF of the network is close to v_0 because the feedback from extrastriate cortex is too small to change the ResF in V1. For a large stimulus whose size is bigger than the range of extrastriate connections, the strong feedback drives the ResF to the value of v (as in Section IV).

6 Discussion

LFP and the activity of local population of neurons In relating our models to local field potential (LFP) measurements, we assumed that the LFP represents the activity of a local population of neurons in cortex. The basis for this
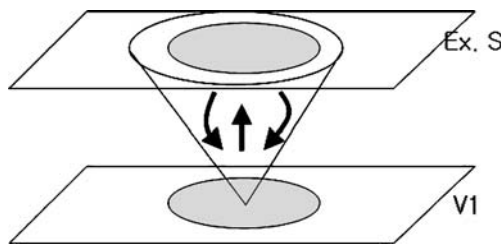

Fig. 10 A Schematic view of a neuron in V1 receiving feedback from extrastriate cortex (labeled Ex. S.). The regions shaded in gray represent active populations of neurons. The Cone shape represents the area where a neuron in V1 has synaptic connections

assumption is the following considerations about the LFP. The LFP is the low frequency (<250 Hz) component of the extracellularly-recorded field potential. Current flows due to synaptic activity dominate these low frequency fluctuations, while currents associated with neuron action potentials dominate higher frequency components (> 300 Hz). The sources of the LFP are thought to be neurons in a sphere of radius 0.5 mm or less (Logothetis et al. 2001; Kruse and Eckhorn 1996). Fluctuations in the LFP are highly correlated with simultaneously measured intracellular voltage fluctuations that are synaptically driven (e.g. Steriade et al. 1996; McCormick et al. 2003; Penttonen et al. 1998; Hasenstaub et al 2005). This observation supports our assumption of a link between the LFP and neuronal population activity.

Resonance and γ-band oscillations in cortex We studied resonant damped oscillations of neuronal activity in a model of V1 and found how cortical interactions determine the ResF and τ_{damp} of the model. We found that the ResF is in the γ-band if the local recurrent excitatory synapses have the kinetics of glutamate AMPA receptors. The resonance is caused by delayed inhibitory feedback from inhibitory neurons to excitatory neurons in our model (as in Freeman 1975; Leung 1982; Rennie et al. 2000). The ResF increases when the strength of the inhibitory cortical feedback loop is strengthened. When self-excitation and self-inhibition feedback loops are made stronger, the ResF decreases. We found that the ResF and the sharpness of the resonant peak of the stimulus-driven response of our network model depends on the size of the stimulus because a larger stimulus activates neurons in a wider area of V1 cortex and that causes cortical feedback from extrastriate cortex to V1 to increase.

There have been other ideas proposed for the source of γ-band oscillations in neural networks. There have been proposals equivalent or identical to our proposal of resonance in a recurrent excitatory-inhibitory circuit (Freeman 1975; Leung 1982; Rennie et al. 2000). But there also have been suggestions for neuronal oscillators in purely inhibitory networks that becomes synchronized in the presence of a tonic excitatory drive (Traub et al. 1996). The resonance model is attractive because it can account for spectral peaks in population activity when individual neurons in the population are only weakly coherent with the population (and LFP) as is often observed *in vivo* (Brunel and Wang 2003; Zeitler et al. 2006; Henrie and Shapley 2005; Montgomery and Buzsaki 2007). The resonance model for gamma band peaks is also consistent with analysis of temporal autocoherence in the LFP (Burns et al. 2008). If the gamma band peak were a result of a neural oscillator as has been hypothesized before (e.g. Traub et al. 1996), then one would expect temporal phase

coherence to extend over long time periods. However, our resonant model driven by stochastic inputs would predict that coherence in the gamma band would be low, and this is what was found by analyzing the autocoherence of the LFP in V1 cortex (Burns et al. 2008). Recent experimental results that employed genetic techniques to stimulate inhibitory interneurons selectively in somatosensory cortex (Cardin et al. 2009) support our theoretical result that gamma-band peaks in the LFP spectrum are a consequence of resonance in the local cortical circuit.

Cortical sharpening of orientation tuning in V1 and the ResF In our previous work (Kang et al. 2003), we found that a V1 neural network can sharpen the orientation tuning of LGN input in two different ways: an untuned-inhibitory mechanism and a tuned-inhibitory, Mexican-hat mechanism. For the untuned-inhibitory mechanism, the inhibitory feedback loop is stronger than self-excitation. For the tuned-inhibitory, Mexican-hat mechanism, the inhibitory feedback loop is more balanced with excitatory feedback. It is difficult to explain the experimental data on LFP power spectra in V1 cortex with a Mexican-hat mechanism. The ResF for the Mexican-hat mechanism is too low compared to the experimentally measured γ-band peak in the LFP power spectrum. The fact that increasing stimulus size shifts the peak of the power spectrum in the γ-band requires that local inhibitory feedback, $S_{EI}S_{IE}$, must be large compared to local excitatory feedback, S_{EE}, consistent with the inhibition-dominated scenario and not the Mexican-hat balanced scenario. The implication is that the sharpening of orientation-tuning in V1 is a consequence of the untuned-inhibition mechanism. Thus, analysis of LFP fluctuations can be used to decide between different cortical network models that were devised to explain orientation selectivity. It is worth mentioning that models of V1 without visual driven inhibition, such as the modified feedforward model in the work of Priebe and Ferster (2008), do not account for the peaks in the visually-driven LFP power spectrum observed in V1 cortex. Also worth noting is the wealth of evidence for visually driven inhibition in V1 (e.g. Volgushev et al. 1993; Borg-Graham et al. 1998; Hirsch et al. 1998); this evidence supports a basic assumption of the V1 model.

6.1 Neural coding and oscillation frequency

Oscillations are thought to play an important role in information processing in the brain (Steriade 2001; Buzsaki 2006). Oscillations in the γ-band (25–90 Hz) have been suggested to represent signals for temporal encoding and stimulus-binding in the visual cortex (Eckhorn et al. 1988; Gray et al. 1989; Womelsdorf et al. 2007). Synchronized retinal oscillations encode essential information that could

be used in escape behavior in frogs (Ishikane et al. 2005). Gamma oscillations appear to couple hippocampal CA3 and CA1 regions dynamically during memory-task performance (Montgomery and Buzsaki 2007). Neuronal coherence could be a mechanism to control the strength of neuronal interaction (Womelsdorf et al. 2007). For example, two simultaneously presented stimuli could be selected based on oscillation frequencies inherent to each stimulus (Borgers and Kopell 2008). Belitski et al. showed how the power of LFPs at different frequencies represents the visual features in the color movies (Belitski et al. 2008). Mazzoni et al. simulated a sparsely connected network of excitatory and inhibitory neurons to determine how LFPs generated by the network encode information about input stimuli (Mazzoni et al. 2008). What we propose in this paper is that γ-band peaks in the power spectrum of cortical network activity are the consequences of resonance in the cortical network. Our study suggests a possible mechanism to control the characteristic oscillation frequency of a neural circuit. The ResF in a recurrent cortical network with feedback, as in V1, could be controlled by threshold nonlinearities. Changing the effective strength of the feedback connections changes the shape of the power spectrum of LFP.

6.2 More realistic models of V1

More realistic network models of V1 could be designed. For example, conduction delay time was ignored in our model. Robinson used a propagator method to study the generation of Gamma oscillation in a network assuming that the cortical interaction is governed by damped wave equations (Robinson 2006). He used a difference-of-exponential model for the time course of conductance change and included conduction delay time. Robinson show that his system can generate Gamma oscillations and that noticeable spectral peaks are created by resonance. But due to the complexity of the model, it is not easy to understand how the power spectrum depends on the parameters of the model. The structure of the network interaction is exactly periodic in the Robinson (2006) model. It is not clear how important this assumption is in general, either.

Schwabe et al. (2006) suggested that a high threshold/high gain local interneuron is innervated and activated by horizontal connections. Surround suppression is explained by such high threshold interneurons in their model. If we included such high threshold neurons in our model, the peak position of the power spectrum might depend on the contrast of the stimulus because the activation of high threshold interneuron at higher contrasts should change the effective total strength of synaptic connections. In fact, contrast dependence of the power spectrum was experimentally observed (Henrie and Shapley 2005).

Here, we used a relatively simple model of V1 to understand the relation between cortical feedback and the power spectrum of neural activity in V1. For instance we have not included nonlinear intrinsic properties of neurons, such as voltage-gated ionic channels, in our model. Studying more realistic models is not necessarily better in understanding the mechanism underlying the observed power spectrum of LFP. Numerical study as well as analytical study is difficult for complicated, more realistic, models and one would have to include in such models unknown parameters and assumptions whose meaning is not clear. In the future as we learn more about cortical neurons and networks, we hope that our model can be made more realistic, and that our study will provide a guideline for the parameter sets to be used for more elaborate models.

Appendix A

Rate equation and time course of conductance change

Consider the time evolution of conductance for AMPA receptors in a neuron. This can be described by an integral. $m(t) = \int A_E(t-a)f_E(a)da$. $f_E(t)$ is $\sum_j \delta\left(a - t_j^i\right)$ where t_j^i is ith spikes from jth presynaptic excitatory neurons and $\delta(t)$ is a delta function. $A_E(t)$ is the time course of conductance change of AMPA receptors. The conductance due to GABA$_A$ receptors, $n(t)$ can be described with another function, $A_I(t)$ in the similar way.

When the number of presynaptic neurons is large and the neural network is in an asynchronous state, $f_E(t)$ can be replaced by the mean firing rate of presynaptic neurons, $\overline{f}_E(t)$ and the mean firing rates are determined by the conductances of the presynaptic neurons: $\overline{f}_E(t) = \overline{f}_E(m(t), n(t), I(t))$ where $I(t)$ is the feed-forward input to the network. Self-consistency requires that $m(t)$ and $n(t)$ should satisfy the following integral equations.

$$m(t) = \int_{-\infty}^{t} A_E(t-a)\overline{f}_E(m(a), n(a), I(a))da \quad \text{(A.1)}$$

$$n(t) = \int_{-\infty}^{t} A_I(t-a)\overline{f}_I(m(a), n(a), I(a))da \quad \text{(A.2)}$$

Once we have the solution of the above integral equations, the firing rate of neurons is given by the time derivative of $m(t)$ and $n(t)$. But an integral equation is difficult to analyze and we simplify the integral equations with two approximations. First, we transform the integral equations into differential equations assuming that explicit

forms of $A_E(t)$ and $A_I(t)$ are given. For example, for an exponential model, $A_E(t) = \exp(-t/\tau_E)/\tau_E$,

$$\tau_E \frac{dm(t)}{dt} = -m(t) + \overline{f}_E(t). \quad \text{(A.3)}$$

where τ_E is the decay time constant of the conductance. For AMPA, τ_E is a few milliseconds. while for NMDA, τ_E is 50–100 msec.

For the difference of exponential model (DOE) with time delay, $A_E(t) = \left(e^{-(t-\delta)/\tau_E} - e^{-(t-\delta)/\tau_{E0}}\right)/(\tau_E - \tau_{E0})$, we find

$$\tau_{E0} \frac{dm(t)}{dt} = -m(t) + m_0(t) \quad \text{(A.4)}$$

$$\tau_E \frac{dm_0(t)}{dt} = -m_0(t) + f_E(t - \delta) \quad \text{(A.5)}$$

where δ is the synaptic delay time, and τ_{E0} is the rising time constant of the conductance's time course. For small τ_{E0}, Eq. A.4 and A.5 can be merged into one equation.

$$\tau_E \frac{dm(t)}{dt} = -m(t) + f_E(t - \delta - \tau_{E0}) \quad \text{(A.6)}$$

Another approximation that achieves the same result as Eq. 1.0 is to assume an explicit form of the mean firing rate, $f_E(t) = f_E(m(t), n(t), I(t))$. The linear form with rectifying nonlinearity is known to be a good approximation for conductance based model neurons (Shriki et al. 2003). When the firing rate fluctuates with small amplitude, a series expansion of firing rate in terms of synaptic conductance variables gives us a linear form as well (Brunel and Wang 2003). See also Shelley and McLaughlin (2002) for a coarse-grained reduction of an integrate-and-fire, conductance-based neural network model to a rate model.

Appendix B

Eigenvalue and ResF with feedback from extrastriate cortex

The characteristic equation of the matrix A in Eq. 3.3 is

$$Det(\lambda I - A) = \lambda^3 - TrA\lambda^2 + R\lambda - DetA = 0 \quad \text{(B.1)}$$

$$TrA = \tau_E^{-1}(1 - S_{EE}) + \tau_I^{-1}(1 + S_{II}) + \tau_{EE}^{-1} \quad \text{(B.2)}$$

$$\begin{aligned} R = &\tau_E^{-1}\tau_I^{-1}((1 - S_{EE})(1 + S_{II}) + S_{EI}S_{IE}) \\ &+ \tau_E^{-1}\tau_{EE}^{-1}(1 - S_{EE} - U_{EF}U_{FE}) \\ &+ \tau_{EE}^{-1}\tau_I^{-1}(1 + S_{II}) \end{aligned} \quad \text{(B.3)}$$

$$\begin{aligned} DetA = &\tau_E^{-1}\tau_I^{-1}\tau_{EE}^{-1} \\ &((1 - S_{EE} - U_{FE}U_{EF})(1 + S_{II}) + S_{EI}S_{IE} + S_{EI}U_{IF}U_{FE}) \end{aligned} \quad \text{(B.4)}$$

The conditions for Eq. B.1 to have eigenvalues with positive real part can be obtained by the Routh-Hurwitz theorem (Weisstein). But here we use a different derivation showing the stability conditions in Eq. 4.2–4 explicitly. The three eigenvalues are either three real numbers or one real number and two complex conjugates. In any case, $TrA > 0$ if the real parts of all eigenvalues are positive. When one of the real eigenvalues changes in sign from positive to negative, $DetA$ is 0 because $DetA$ is the product all eigenvalues. It means $DetA > 0$. Finally, when the real parts of two complex eigenvalues change their sign, the three eigenvalues have the form $\varepsilon \pm \alpha i$ and β where ε, α and β are three real numbers. It is easy to prove the following using the relation between roots and coefficients of the equation.

$$TrA = 2\varepsilon + \beta, \tag{B.5}$$

$$R = \varepsilon^2 + \alpha^2 + 2\varepsilon\beta, \tag{B.6}$$

$$DetA = (\varepsilon^2 + \alpha^2)\beta, \tag{B.7}$$

$$TrA*R - DetA = (2a^2 + 2b^2)\varepsilon + O(\varepsilon^2) \tag{B.8}$$

Therefore, the conditions for the real parts of all eigenvalues to be positive are given in the following way.

$$TrA > 0 => \tau_E^{-1}(1 - S_{EE}) + \tau_I^{-1}(1 + S_{II}) + \tau_{EE}^{-1} > 0 \tag{B.9}$$

$$DetA > 0 => (1 - S_{EE} - U_{FE}U_{EF})(1 + S_{II}) \\ + S_{EI}S_{IE} + S_{EI}U_{IF}U_{FE} > 0 \tag{B.10}$$

$$TrA*R > DetA => T\left(\tau_E^{-1}\tau_I^{-1}D + \tau_{EE}^{-1}T + \tau_{EE}^{-2}\right) \\ - \tau_E^{-1}\tau_I^{-1}\tau_{EE}^{-1}S_{EI}U_{IF}U_{FE} \\ - \tau_E^{-1}\tau_{EE}^{-1}\left(\tau_{EE}^{-1} + \tau_E^{-1}(1 - S_{EE})\right) \\ U_{EF}U_{FE} > 0. \tag{B.11}$$

where $T = \tau_E^{-1}(1 - S_{EE}) + \tau_I^{-1}(1 + S_{II})$ and $D = (1 - S_{EE})(1 + S_{II}) + S_{EI}S_{IE}$.

When $TrA^*R = DetA$, the real part of the complex eigenvalues are zero and $R = DetA/TrA = (2\pi v)^2$.

Since is proportional to the inverse of the real part of the eigenvalue, $\tau_{damp} = \infty$ on the stability line defined by the Eq. B.11. Equation B.6 shows that $R = DetA/TrA = (2\pi v)^2$ in this case. Then the ResF, v obeys

$$(2\pi v)^2 = \left(T + \tau_{EE}^{-1}\right)^{-1}\tau_E^{-1}\tau_I^{-1}\tau_{EE}^{-1} \\ (D + S_{EI}U_{IF}U_{FE} - (1 + S_{II})U_{FE}U_{EF}) \tag{B.12}$$

References

Angelucci, A., Levitt, J. B., Walton, E. J., Hupe, J. M., Bullier, J., & Lund, J. S. (2002). Circuits for local and global signal integration in primary visual cortex. *Neuroscience, 22,* 8633–8646.

Belitski, A., Gretton, A., Magri, C., Murayama, Y., Montemurro, M. A., Logothetis, N. K., et al. (2008). Low-Frequency Local Field Potentials and Spikes in Promary Visul Cortex Convey Independent Visual Information. *Journal of Neuroscience, 28,* 5696–709.

Ben-Yishai, R., Bar-Or, R., & Sompolinsky, H. (1995). Theory of orientation tuning in visual cortex. *Proceedings of the National Academy of Sciences of the United States of America, 92,* 3844–3848.

Borg-Graham, L. J., Monier, C., Frégnac, Y. (1998). Visual input evokes transient and strong shunting inhibition in visual cortical neurons. *Nature, 393*(6683), 369–73.

Borgers, C., & Kopell, N. J. (2008). Gamma oscillation and stimulus selection. *Neural Computation, 20,* 383–414.

Brunel, N., & Wang, X. J. (2003). What determines the frequency of fast network oscillations with irregular neural discharges? I. Synaptic dynamics and excitation-inhibition balance. *Journal of Neurophysiology, 90,* 415–430.

Burns, S. P., Shapley, R. M., Shelley, M. J., & Xing, D. (2008). Searching for phase coherence in the cortical network with time-frequency analysis of the local field potential. *Society for Neuroscience Abstracts, 38,* 163.4.

Buzsaki, G. (2006). *Rhythms of the brain*. New York: Oxford UP.

Cardin, J. A., Carlén, M., Meletis, K., Knoblich, U., Zhang, F., Deisseroth, K., et al. (2009). Driving fast-spiking cells induces gamma rhythm and controls sensory responses. *Nature, 459*(7247), 663–7.

Eckhorn, R., Bauer, R., Jordan, W., Brosch, M., Kruse, W., Munk, M., et al. (1988). Coherent oscillations: a mechanism of feature linking in the visual cortex? Multiple electrode and correlation analyses in the cat. *Biological Cybernetics, 60,* 121–130.

Eckhorn, R., Frien, A., Bauer, R., Woelbern, T., Kehr, H. (1993). High frequency (60–90 Hz) oscillations in primary visual cortex of awake monkey. *Neuroreport, 4*(3), 243–6.

Freeman, W. J. (1975). *Mass action in the nervous system*. New York: Academic.

Gieselmann, M. A., & Thiele, A. (2008). Comparison of spatial integration and surround suppression characteristics in spiking activity and the local field potential in macaque V1. *European Journal of Neuroscience, 28,* 447–459.

Goldberg, J. A., Rokni, U., & Sompolinsky, H. (2004). Patterns of Ongoing Activity and the Functional Architectureof the Primary Visual Cortex. *Neuron, 42,* 489–500.

Gonchar, Y., & Burkhalter, A. (2003). Distinct GABAergic targets of feedforward and feedback connections between lower and higher areas of rat visual cortex. *Journal of Neuroscience, 23,* 10904–12.

Gray, C. M., Konig, P., Engle, A. K., & Singer, W. (1989). Oscillatory responses in cat visual cortex exhibit inter-columnar synchronization which reflects global stimulus properties. *Nature, 338,* 334–337.

Hasenstaub, A., Shu, Y., Haider, B., Kraushaar, U., Duque, A., & McCormick, D. A. (2005). Inhibitory postsynaptic potentials carry synchronized frequency information in active cortical networks. *Neuron, 47*(3), 423–35.

Henrie, J. A., & Shapley, R. (2005). LFP power spectra in V1 cortex: the graded effect of stimulus contrast. *Journal of Neurophysiology, 94*(1), 479–90.

Henrie, J. A., Kang, K., & Shapley, R. (2005). Stimulus size affects the LFP spectral contents in primate V1. *Society for Neuroscience Abstracts, 35,* 284.18.

Hirsch, J. A., Alonso, J. M., Reid, R. C., & Martinez, L. M. (1998). Synaptic integration in striate cortical simple cells. *Journal of Neuroscience, 18,* 9517–28.

Ishikane, H., Gangi, M., Honda, S., & Tachibana, M. (2005). Synchronized retinal oscillations encode essential information for escape behavior in frogs. *Nature Neuroscience, 8*(8), 1087–95.

Kang, K., Shelley, M. J., & Sompolinsky, H. (2003). Mexican hats and pinwheels in visual cortex. *Proceedings of the National Academy of Sciences of the United States of America, 100*(5), 2848–2853.

Kruse, W., & Eckhorn, R. (1996). Inhibition of sustained gamma oscillations (35–80 Hz) by fast transient responses in cat visual cortex. *Proceedings of the National Academy of Sciences of the United States of America, 93*, 6112–6117.

Leung, L. S. (1982). Nonlinear feedback model of neuronal populitons in hippocampal CA1 region. *Journal of Neuophysiology, 47*, 845–868.

Logothetis, N. K., Pauls, J., Augath, M., Trinath, T., & Oeltermann, A. (2001). Neurophysiological investigation of the basis of the fMRI signal. *Nature, 412*(6843), 150–7.

Lund, J. S. (1988). Anatomical organization of macaque monkey striate visual cortex. *Annual Reviews of Neuroscience, 11*, 253–88.

Lund, J. S., Angelucci, A., & Bressloff, P. C. (2003). Anatomical substrates for functional columns in macaque monkey primary visual cortex. *Cerebral Cortex, 13*, 15–24.

Mazzoni, A., Panzeri, S., Logothetis, N. K., & Brunel, N. (2008). Encoding of Naturalistic Stimuli by Local Field Potential Spectra in Networks of Excitatory and Inhibitory Neurons. *PLOS Computational Biology, 4*, e10000239.

McCormick, D. A., Shu, Y., Hasenstaub, A., Sanchez-Vives, M., Badoual, M., & Bal, T. (2003). Persistent cortical activity: mechanisms of generation and effects on neuronal excitability. *Cerebral Cortex, 13*(11), 1219–31.

McLaughlin, D., Shapley, R., Shelley, M., & Wielaard, J. (2000). A neuronal network model of macaque primary visual cortex (V1): orientation selectivity and dynamics in the input layer 4Calpha. *Proceedings of the National Academy of Sciences of the United States of America, 97*, 8087–8092.

Montgomery, S. M., & Buzsáki, G. (2007). Gamma oscillations dynamically couple hippocampal CA3 and CA1 regions during memory task performance. *Proceedings of the National Academy of Sciences of the United States of America, 104*(36), 14495–500.

Penttonen, M., Kamondi, A., Acsady, L., & Buzsaki, G. (1998). Gamma frequency oscillation in the hippocampus of the rat: intracellular analysis *in vivo*. *European Journal of Neuroscience, 10*(2), 718–28.

Priebe, N. J., & Ferster, D. (2008). Inhibition, spike threshold, and stimulus selectivity in primary visual cortex. *Neuron, 57*, 482–97.

Rennie, C. J., Wright, J. J., & Robinson, P. A. (2000). Mechanisms of Cortical Electrical Activity and Emergence of Gamma Rhythm. *Journsl of Theoretical Biology, 205*, 17–35.

Ringach, D. L., Hawken, M. J., & Shapley, R. (1997). Dynamics of orientation tuning in macaque primary visual cortex. *Nature (London), 387*, 281–284.

Robinson, P. A. (2006). Patch propagators, brain dynamics, and the generation of spatially structured gamma oscillation. *Physical Review E, 73*, 041904.

Schwabe, L., Obermayer, K., Angelucci, A., & Bressloff, P. C. (2006). The role of feedback in shaping the extra-classical receptive field of cortical neurons: a recurrent network model. *Journal of Neuroscience, 26*(36), 9117–29.

Shelley, M., & McLaughlin, D. (2002). Coarse-grained reduction and analysis of a network model of cortical response: I. Drifting grating stimuli. *Journal of Computer Neuroscience, 12*(2), 97–122.

Shriki, O., Hansel, D., & Sompolinsky, H. (2003). Rate models for conductance-based cortical neuronal networks. *Neural Computation, 15*(8), 1809–41.

Somers, D., Nelson, S., & Sur, M. (1995). An emergent model of orientation selectivity in cat visual cortical simple cells. *Journal of Neuroscience, 15*, 5448–5465.

Steriade, M. (2001). *Intact and Sliced Brain*. Cambridge: MIT.

Steriade, M., Amzica, F., & Contreras, D. (1996). Synchronization of fast (30–40 Hz) spontaneous cortical rhythms during brain activation. *Journsl of Neuroscience, 16*, 392–417.

Tao, L., Cai, D., McLaughlin, D. W., Shelley, M. J., & Shapley, R. (2006). Orientation selectivity in visual cortex by fluctuation-controlled criticality. *Proceedings of the National Academy of Sciences of the United States of America, 103*(34), 12911–6.

Traub, R., Whittington, M. A., Stanford, I. M., & Jefferys, J. G. R. (1996). Gap junctions between interneuron dendrites can enhance synchrony of gamma oscillations in distributed networks. *Journal of Neuroscience, 21*, 9478–9486.

Troyer, T., Krukowski, A., Priebe, N., & Miller, K. (1998). Contrast-invariant orientation tuning in cat visual cortex: thalamocortical input tuning and correlation-based intracortical connectivity. *Journal of Neuroscience, 18*, 5908–5927.

Volgushev, M., Pei, X., Vidyasagar, T. R., & Creutzfeldt, O. D. (1993). Excitation and inhibition in orientation selectivity of cat visual cortex neurons revealed by whole-cell recordings *in vivo*. *Visual Neuroscience, 10*, 1151–5.

Weisstein, E. W. Routh-Hurwitz Theorem. From MathWorld—A Wolfram Web Resource. http://mathworld.wolfram.com/Routh-HurwitzTheorem.html.

Womelsdorf, T., Schoffelen, J. M., Oostenveld, R., Singer, W., Desimone, R., Engel, A. K., et al. (2007). Modulation of neuronal interactions through neuronal synchronization. *Science, 316*, 1609–12.

Zeitler, M., Fries, P., Gielen, S. (2006). Assessing neuronal coherence with single-unit, multi-unit, and local field potentials. *Neural Computation, 18*(9), 2256–81.